This is the peer-reviewed, final accepted version for American Mineralogist, published by the Mineralogical Society of America.
The published version is subject to change. Cite as Authors (Year) Title. American Mineralogist, in press.
DOI: https://doi.org/10.2138/am-2022-8696. http://www.minsocam.org/

Word Count: 3423

Revision 1

The equilibrium boundary of the reaction $Mg_3Al_2Si_3O_{12} + 3CO_2 = Al_2SiO_5 + 2SiO_2 + 3MgCO_3$ at 3-6 GPa

Yulia G. Vinogradova[1], Anton Shatskiy[1*], Anton V. Arefiev[1], Konstantin D. Litasov[2]

[1]Vernadsky Institute of Geochemistry and Analytical Chemistry of the Russian Academy of Science, Moscow 119991, Russia

[2]Vereshchagin Institute for High Pressure Physics of the Russian Academy of Science, Troitsk, Moscow, 108840, Russia

*telephone: +7 (913) 385 6129, e-mail: shatskiy@geokhi.ru

Abstract

The stability of CO_2 fluid in the Earth's mantle is restricted by the carbonation of rock-forming minerals. Among those, the reaction with garnet is of particular interest because it constrains the stability of CO_2 fluid in eclogites, whose minerals have been found in the CO_2-bearing diamonds. In this work, we determined the equilibrium boundary for the reaction $Mg_3Al_2Si_3O_{12}$ (Prp) + $3CO_2$ (F) = Al_2SiO_5 (Ky) + $2SiO_2$ (Coe/Qz) + $3MgCO_3$ (Mgs) over the pressure interval 3-6 GPa using a multianvil press. Owing to the slow kinetics, the reaction was studied in both forward (left to right) and reverse (right to left) directions in experiments with durations extending up to 260 h. Our newly determined boundary is situated 3 GPa / 950±50 °C, 4.5 GPa / 1075±25 °C, and 6 GPa / 1250±50 °C and has the equation P(GPa) = 0.0099×T (°C) + 6.3165. The boundary crosses the

This is the peer-reviewed, final accepted version for American Mineralogist, published by the Mineralogical Society of America.
The published version is subject to change. Cite as Authors (Year) Title. American Mineralogist, in press.
DOI: https://doi.org/10.2138/am-2022-8696. http://www.minsocam.org/

graphite-to-diamond transition curve near 4.5 GPa and 1100 °C. Thus, the assemblage garnet + CO_2 fluid is stable in the diamond stability field under *P-T* conditions of the continental geotherm with a heat flow of 40 mW/m^2.

Keywords: CO_2 fluid, pyrope, carbonation, garnet, phase relations, high pressure, multianvil experiments, Earth's mantle

Nomenclature			
Alm	almandine	Fo	forsterite
Carb	carbonate	Gr	graphite
Coe	coesite	Grs	grossular
Cpx	clinopyroxene	Grt	garnet
Crn	corundum	Ky	kyanite
Di	diopside	Mgs	magnesite
Dia	diamond	Opx	orthopyroxene
Dol	dolomite	Prp	pyrope
En	enstatite	Qz	quartz
F	fluid	Sd	siderite

Introduction

The presence of CO_2 fluid during crystallization of some lithospheric diamonds is evidenced by findings of solid (Schrauder and Navon 1993; Chinn 1995; Barannik et al. 2021) and liquid CO_2 (Tomilenko et al. 2001; Smith et al. 2015) inclusions in natural diamonds. Systematic studies of CO_2-bearing diamonds revealed inclusions of eclogitic minerals (Chinn 1995; Ragozin et al. 2002; Ragozin et al. 2009). However, the stability of CO_2 in the diamond stability field in eclogites (besides redox conditions) is restricted by carbonation reactions of clinopyroxene and garnet (Hammouda and Keshav 2015) (Fig. 1).

It was experimentally shown, that clinopyroxene in the case of pure diopside is unstable with CO_2 in the *P-T* range of diamond stability (Luth 1995; 2006). However, the addition of iron to

clinopyroxene expands its stability to the *P-T* conditions of lithospheric diamond formation (Martin and Hammouda 2011) (Fig. 1).

For a long time, conclusions about garnet stability with CO_2 were based on the work by Knoche et al. (1999) in which the reaction boundary:

$$Mg_3Al_2Si_3O_{12}\,(Prp) + 3CO_2 = 3MgCO_3\,(Mgs) + Al_2SiO_5\,(Ky) + 2SiO_2\,(Coe), \quad (1)$$

is situated at higher temperatures than most estimates for lithospheric diamond formation (Shirey et al. 2013; Stachel and Luth 2015) (Fig. 1). In the study by Knoche et al. (1999), several starting mixtures were employed. The most robust results were obtained using the oxide-carbonate starting mixture in experiments at 5.2 and 7.5 GPa and a duration of 4-6 h (Fig. 2a).

Recently, Bataleva et al. (2020b) reported new experimental data on the reaction boundary. They also used the oxide-carbonate starting mixture but in longer experiments with a duration extending up to 10-60 h (Fig. 2a). A comparison of these two studies shows that the reaction boundary shifts to lower temperatures as the run duration increases (Fig. 2). These observations and low conversion of the initial reagents into garnet indicate slow kinetics of the decarbonation reaction. Since in both works, the reaction was mainly studied only in the decarbonation direction, the established reaction boundaries may deviate to higher temperatures relative to the equilibrium one owing to slow kinetics.

In order to exclude kinetic factors and determine the equilibrium boundary, we have investigated the reaction in both carbonation and decarbonation directions in multianvil experiments at 3-6 GPa, 900-1500 °C, and a duration of up to 260 h.

Experimental procedure

Two starting materials were employed to study the reaction from both sides. The first one (A) is a sandwich of natural pyrope powder, $Mg_{2.95}Fe_{0.05}Al_2Si_3O_{12}$, and $Ag_2C_2O_4$ as a CO_2 source. The

second one (B) is a mixture of reagent grade SiO_2, Al_2O_3, and natural magnesite (< 0.1% impurities) from Brumado (Bahia, Brazil), blended in a molar ratio of 3:1:3. Prior to mixing the oxides were annealed at 1000 °C and magnesite at 300 °C for 1 hour.

Experiments were run using a DIA-type 1500-ton press. Eight tungsten carbide cubes with 12-mm truncations were employed as anvils of the inner stage. Octahedra with an edge length of 20.5 mm with ground edges and corners made of semisintered CaO-doped ZrO_2 ceramics (Shatskiy et al. 2010) were employed as pressure media. The high temperature was generated using a tubular graphite heater 4.0/4.5 mm in inner/outer diameter and 11 mm in length. The samples were loaded in graphite or platinum capsules insulated from the heater by a MgO-SiO_2 sleeve made of talc fired at 1000 °C for 1 h. The temperature was monitored with a W97%Re3%-W75%Re25% thermocouple inserted through the heater walls and electrically insulated by Al_2O_3 tubes. No pressure correction on emf was applied. A pressure calibration was performed by monitoring the resistance changes in Bi at 2.5 and 7.7 GPa at room temperature and using known phase transitions in SiO_2 (quartz-coesite) and $CaGeO_3$ (garnet-perovskite) at 1100 °C (Shatskiy et al. 2018).

High-pressure cells with oxide-carbonate mixtures were dried for 1 night at 200 °C in a vacuum furnace just before the experiment. The cells containing samples with $Ag_2C_2O_4$ were prepared just before the experiment and loaded in the press without drying to avoid oxalate decomposition.

Experiments were performed by compression to a desirable load (3-6.5 MN) at a rate of 1 MN/h, heating to the target temperature at a rate of 50 °C/min and maintenance within 2 °C of the desired value in a temperature control mode. After the required time, the power was turned off, resulting in a temperature drop to <100 °C in 10 s, followed by decompression at a rate of 1 MN/h.

The recovered samples were mounted into epoxy, ground in an axial direction using sandpapers, and polished using a 3-μm diamond paste. After sample cleaning in benzene and carbon

This is the peer-reviewed, final accepted version for American Mineralogist, published by the Mineralogical Society of America.
The published version is subject to change. Cite as Authors (Year) Title. American Mineralogist, in press.
DOI: https://doi.org/10.2138/am-2022-8696. http://www.minsocam.org/

coating, the samples were analyzed with MIRA 3 LMU scanning electron microscope (Tescan Orsay Holding, Brno-Kohoutovice, Czech Republic), coupled with an INCA energy-dispersive X-ray micro-analysis system 450. Raman spectra for SiO_2 were collected on a Horiba Jobin Yvon LabRAM HR800 Raman microspectrometer with the 532.1 nm solid-state laser.

Experimental results

The starting material $Mg_3Al_2Si_3O_{12}$ + $Ag_2C_2O_4$

At 6.0 GPa / 1100, 1200 °C, 4.5 GPa / 950-1050 °C, and 3.0 GPa / 900 °C in the starting mixture A, initial pyrope reacts with CO_2 to form kyanite, coesite, and magnesite (Figs. 3, 4a-j, 5, Table 1). The reaction was established in graphite and Pt capsules (Fig. 4a, d, f, h). Newly formed phases are represented by a granular aggregate at the interface between pyrope and silver, formed as a result of $Ag_2C_2O_4$ decomposition (Fig. 4b, e, g, i, j). At 1100, 1200 °C and 6 GPa, coesite and kyanite form short prismatic crystals, while magnesite forms isometric crystals up to 10 μm in size (Fig. 4c, e). The grain size of the newly formed phases at lower temperatures does not exceed 5 μm (Fig. 4g, i, j). Kyanite forms needle-shaped crystals in the magnesite matrix, while coesite forms irregular-shaped clusters (Fig. 4 i, j).

As temperature increases to 1200 °C at 4.5 GPa and 1000, 1100 °C at 3 GPa, the reaction between pyrope and CO_2 has run to completion. The samples are represented by an aggregate of pyrope crystals, 20-50 μm in size, with rounded irregular shape and layers of metallic silver (Fig. 4k, l). No newly formed phases appear at the pyrope-silver interface (Fig. 4l). The pyrope aggregate contains voids, the size and number of which are greatest near the boundary with silver. Besides, the pyrope crystals also contain numerous round voids with a size of 1-2 μm (Fig. 4l). The observed voids indicate the presence of CO_2 fluid during garnet recrystallization. The absence of newly

This is the peer-reviewed, final accepted version for American Mineralogist, published by the Mineralogical Society of America.
The published version is subject to change. Cite as Authors (Year) Title. American Mineralogist, in press.
DOI: https://doi.org/10.2138/am-2022-8696. http://www.minsocam.org/

formed phases indicates that pyrope is thermodynamically stable with CO_2 fluid under given *P-T* conditions.

The starting material $3SiO_2 + Al_2O_3 + 3MgCO_3$

At 6.0 GPa / 1100, 1200 °C and 4.5 GPa / 950-1050 °C, the samples in both Pt and graphite capsules are represented by an aggregate of coesite, kyanite, and magnesite crystals with a grain size of 5-15 μm (Figs. 3, 6a-b, Table 1).

As temperature increases to 1300-1500 °C at 6.0 GPa, 1100-1250 °C at 4.5 GPa, and 1000-1100 °C at 3 GPa pyrope is formed (Fig. 3, Table 1). At 4.5 and 6 GPa, the high-temperature samples are mainly represented by a porous aggregate of pyrope crystals (Fig. 6c, d), while as temperature decreases the fraction of residual kyanite, coesite, and magnesite increases (Fig. 6f-g). Pyrope forms irregularly shaped grains with roundish outlines 20-50 μm in size. The grains contain round voids 1-3 μm in size (Fig. 6e). Numerous round voids within crystals and in the intergranular space indicate the presence of CO_2 fluid. No melting occurs in the entire *P-T* range up to 1500 °C and 6 GPa (Fig. 6c-e).

At 3.0 GPa, 1000 and 1100 °C, the samples are represented by a porous aggregate of enstatite, pyrope, corundum, and minor amounts of kyanite ± quartz (Fig. 5a), and magnesite (Fig. 6h-l). At 3.0 GPa and 1100 °C, the sample contains polyphase clusters with concentric zoning. The clusters consist of magnesite core, then enstatite surrounded by garnet and corundum (Fig. 5i). The formation of enstatite proceeds via the reaction:

$$SiO_2\ (Qz) + MgCO_3\ (Mgs) = MgSiO_3\ (En) + CO_2\ (F). \quad (2)$$

Enstatite contains alumina, however, its distribution is very inhomogeneous and varies from pure enstatite to enstatite containing up to 3-5 mol% Al_2O_3. At 3.0 GPa and 1000 °C, irregular-shaped clusters of alumina appear within enstatite aggregate, which also contains inclusions of magnesite

(Fig. 6j-l). Pyrope grows to well-shaped isometric crystals up to 50 μm in size concentrated at the LT sample side (Fig. 6j). Both spongy-textured enstatite and rounded voids in garnet crystals indicate the presence of CO_2 fluid phase during the experiment (Fig. 6h-l). The growth of enstatite in coexistence with corundum (Fig. 6k) in the pyrope stability field (> 1.5-2.0 GPa) is due to a nucleation problem of pyrope, which was pointed out early (Boyd and England 1959).

According to our data at 3.0 GPa, the assemblage En + CO_2 becomes stable at 950 ± 50 °C (Fig. 7). It should be also emphasized that reaction (2) was established in both forward (left to right) and reverse (right to left) directions (Fig. 7). At 900 °C, the formation of coesite and magnesite from the mixture A (pyrope-oxalate) was established (Fig. 4h-j), while at 1000 °C, enstatite with CO_2 was formed from the mixture B (oxide-carbonate) (Fig. 6j-l). The established boundary is ~200 °C cooler than that established by Litasov and Shatskiy (2019) *in situ* at a synchrotron radiation facility (Fig. 6). Considering the longer duration of our quench experiments, 260 h, compared to the *in situ* ones, < 0.5 h, the discrepancy is due to insufficient run duration and the use of low-temperature assembly as a starting mixture in the previous study. It should also be noted that our experiments at 3 GPa and experimental data (Koziol and Newton 1995), obtained by studying the forward and reverse reactions in experiments lasting tens and hundreds of hours, indicate the presence of a kink on the reaction line, which could be associated with the quartz-coesite transformation (Fig. 7). Thus, the slow kinetics of decarbonation reactions imposes restrictions on their study *in situ* using synchrotron radiation at least at temperatures below 1200-1300 °C.

Discussion

Results of the study of the forward reaction (carbonation in the system garnet-oxalate) and the reverse reaction (decarbonation in the system oxide-carbonate) are presented in Fig. 3. As can be seen, the stability fields of the assemblages Grt + CO_2 and Ky + Coe + Mgs, obtained in the oxide-

carbonate system, coincide with those obtained in the pyrope-oxalate system (Fig. 3). Thus, the established position of the reaction boundaries is thermodynamically justified. According to our data, the equilibrium boundary of reaction (1) passes through 3 GPa / 950±50 °C, 4.5 GPa / 1075±25 °C, and 6 GPa / 1250±50 °C with a slope of ~ 10 MPa/°C.

Our and previous results are consistent at high temperatures. The reaction boundaries from different studies converge at around 1400 °C and 7.5 GPa (Fig. 8a). However, at lower pressures, the boundaries from the early studies are situated at higher temperatures than that established here. The largest difference, 170 °C at 4.5 GPa, is observed between our boundary and that of Knoche et al. (1999) established at the run duration of 1-8 h (Fig. 8a). The difference between our results and that obtained by Bataleva et al. (2020b) in experiments with a duration of 10-60 h is smaller, 150 °C at 3 GPa (Fig. 8a). The position of the boundaries from both previous works is based on the study of decarbonation using the oxide-carbonate starting mixture. This explains the shift of these boundaries to higher temperatures compared to the boundary established in this study in the forward and reverse experiments of longer duration, up to 260 h.

In our experiments at 1200 °C and 4.5 GPa, pyrope does not react with CO_2 fluid even after annealing for 25 h. While as temperature decreases to 1050 °C at 4.5 GPa, the Ky + Coe + Mgs assemblage was formed after 166 h (Fig. 4g). Knoche et al. (1999) also conducted experiments in the pyrope-oxalate system at 1000 and 1200 °C and 4.5 GPa with a duration of 8 h but the obtained results are hard to interpret. According to powder XRD, both samples are represented by pyrope and do not contain the carbonation products except for minor magnesite (Fig. 2a).

Besides, Knoche et al. (1999) conducted experiments with an oxide-carbonate-pyrope-oxalate mixture at 6.4 GPa. However, no change in phase composition was observed over the studied temperature range (Fig. 2a). The presence of kyanite, coesite, and magnesite in the starting material should complicate unambiguous detection of newly formed products of the carbonation reaction if

any. On the other hand, the difference in the phase ratio, determined by powder XRD for small high-pressure samples, is ambiguous.

The obtained results are in reasonable agreement with the longer 10-60-h experiments of Bataleva et al. (2020b) conducted at 6.3 and 7.5 GPa (Figs. 2b, 3, 8a). Nevertheless, the results of the low-temperature experiments at 3 GPa are inconsistent (Figs. 2b, 3, 8a). According to the data of Bataleva et al. (2020b) at 3 GPa, the boundary of reaction (1) is located at 1100 °C, which is 150 °C higher than that in our study (Fig. 8a). This difference is probably due to the insufficient run duration in the study by Bataleva et al. (2020b), 60 h at 1050 °C and 3 GPa (Figs. 2b, 3). According to our study at 3 GPa, the decarbonation occurs even at 1000 °C if the duration extends to 260 h. On the other hand, the reverse, carbonation, reaction was established at 900 °C in the experiment with the pyrope-oxalate composition and a duration of 150 h (Fig. 3).

In this study at 3 GPa, silica is represented by quartz at 1000 °C and coesite at 900 °C (Figs. 3, 9). This is consistent with the quartz-to-coesite transition boundary reported by Hemingway et al. (1998). Unlike that, in the study by Bataleva et al. (2020b) at 3 GPa, silica is represented by coesite to at least 1150 °C. In the study by Bataleva et al. (2020b), the high-temperature pressure calibration was done at pressures exceeding 5.5 GPa using the graphite-to-diamond transition (Pal'yanov et al. 2002; Shatskii et al. 2002; Sokol et al. 2015), while the lower pressure, 3 GPa, was calibrated at room temperature. A CsCl-bearing high-pressure cell employed in a split-sphere multi-anvil apparatus (BARS) by Bataleva et al. (2020b) has a significant thermal pressure, similar to a NaCl-bearing pressure medium in a Belt apparatus reported by Fukunaga et al. (1999). A comparison of high-temperature and room-temperature pressure calibrations of BARS yields a 30 % pressure increase with heating (Shatskiy et al. 2011). Therefore, the pressure overestimation may be an alternative cause of the discrepancy in the results at 3 GPa. Given the potential kinetics problem and

the problem with pressure calibration at 3 GPa in Bataleva et al. (2020b), it is possible that the kink on the boundary of reaction (1) suggested in their study is not real.

Despite the differences at 3 GPa, the extrapolation of our data to high pressures coincides with the data of Bataleva et al. (2020b) obtained at 6.3 and 7.5 GPa (Fig. 8a). This is reasonable considering the robust calibration of their experiments at these pressures and the absence of kinetic problems at such high temperatures and durations of experiments. Linear approximation of our data gives the following equation of reaction (1): P(GPa) = 0.0099×T (°C) + 6.3165 (R^2 = 0.9908) (Fig. 8a). The boundary crosses the graphite-to-diamond transition curve (Day 2012) near 4.5 GPa and 1100 °C, which means that the assemblage garnet + CO_2 fluid is stable in the diamond stability field under *P-T* conditions of the continental geotherm with a heat flow of 40 mW/m^2 (Hasterok and Chapman 2011) (Fig. 9).

Implications

It is generally accepted that under mantle *P-T* conditions, reactions involving carbonates proceed quickly and therefore the phase boundaries obtained in short experiments (several hours and even minutes) are equilibrium. In this work, we found that this is not always the case. The study of reaction (1) from both the forward (carbonation) and reverse (decarbonation) directions made it possible to establish an equilibrium boundary, which is located below the boundaries determined earlier in shorter decarbonation experiments (Fig. 8a). We found that at low temperatures of 900-1100 °C at 3-6 GPa, the reaction time achieves 130-260 h. We also found that it is difficult to escape from the slow kinetic problem if the reaction is studied from one side using a low-temperature high-pressure oxide-carbonate assemblage as a starting mixture in the experiments with a duration of less than 100 h. A similar problem can be expected when studying the reactions of CO_2 with garnets of a more complex composition. According to thermodynamic calculations (Knoche et al. 1999;

Bataleva et al. 2020a; Vinogradova et al. 2021), the position of the reaction boundary shifts to lower temperatures in the grossular-pyrope-almandine (Grs-Prp-Alm) series (Fig. 8b). However, the experimentally established reaction boundaries for $Prp_{30}Alm_{70}$ and $Prp_{83}Grs_{17}$ garnets match with the pyrope-CO_2 reaction boundary determined by the same authors (Bataleva et al. 2020a; Bataleva et al. 2020b) at 7.5 and 3 GPa, respectively (Fig. 8). If we compare them with the boundary obtained in the current work, then the boundary $Prp_{30}Alm_{70}$ + CO_2 at 3.0 GPa is situated higher in temperature than that Prp + CO_2, which contradicts the calculations (Fig. 8b). In addition, the Ca/Mg ratio in $Prp_{83}Grs_{17}$ differs from the bulk Ca# 50, which can be a result of incomplete conversion and difference in the reaction rates of Ca and Mg components. Therefore, known data on reactions of garnets and CO_2 requires an experimental refinement with an approach involving both forward (carbonation) and reverse (decarbonation) experiments with a duration exceeding 100-150 h.

The reaction boundary pyrope + CO_2 established in the present experiments is situated at lower temperatures than that determined using thermodynamic calculations (Knoche et al. 1999; Bataleva et al. 2020b; Vinogradova et al. 2021) (Fig. 8a). The difference may be because the calculations do not account for the silicate solute lowering the activity of CO_2 in the fluid phase. We also suspect that at pressures corresponding to the diamond stability field, the upper-temperature limit of the CO_2 fluid stability in equilibrium with garnet of a more complex composition may be limited by partial melting rather than carbonation reaction. This emphasizes the importance of further studies of the stability of CO_2 fluid with garnets of a more complex composition.

Acknowledgments

We are grateful to Oded Navon and Tahar Hammouda for constructive reviews, which improved the manuscript. This work is financially supported by Russian Science Foundation (project No 21-17-00024).

256

257 **References**

258 Barannik, E.P., Shiryaev, A.A., and Hainschwang, T. (2021) Shift of CO_2-I absorption bands in
259 diamond: A pressure or compositional effect? A FTIR mapping study. Diamond and Related
260 Materials, 113, 108280.

261 Bataleva, Y.V., Kruk, A.N., Novoselov, I.D., Furman, O.V., and Palyanov, Y.N. (2020a)
262 Decarbonation reactions involving ankerite and dolomite under upper mantle P, T-
263 parameters: Experimental modeling. Minerals, 10(8), 715.

264 Bataleva, Y.V., Novoselov, I.D., Kruk, A.N., Furman, O.V., Reutsky, V.N., and Palyanov, Y.N.
265 (2020b) Experimental modeling of decarbonation reactions resulting in Mg, Fe-garnets and
266 CO_2 fluid at the mantle P–T parameters. Russian Geology and Geophysics, 61(5-6), 650-
267 662.

268 Boyd, F.R., and England, J.L. (1959) Pyrope. DC, Carnegie Institution of Washington Year Book,
269 58, 83-87.

270 Chinn, I.L. (1995) A study of unusual diamonds from the George Creek K1 Kimberlite dyke,
271 Colorado, PhD thesis. PhD thesis, University of Cape Town, South Africa.

272 Day, H.W. (2012) A revised diamond-graphite transition curve. American Mineralogist, 97(1), 52-
273 62.

274 Fukunaga, O., Ko, Y.S., Konoue, M., Ohashi, N., and Tsurumi, T. (1999) Pressure and temperature
275 control in flat-belt type high pressure apparatus for reproducible diamond synthesis.
276 Diamond and Related Materials, 8(11), 2036-2042.

277 Hammouda, T., and Keshav, S. (2015) Melting in the mantle in presence of carbon: Review of
278 experiments and discussion on the origin of carbonatites. Chemical Geology, 418, 171-188.

279 Hasterok, D., and Chapman, D.S. (2011) Heat production and geotherms for the continental
280 lithosphere. Earth and Planetary Science Letters, 307(1-2), 59-70.
281 Hemingway, B.S., Bohlen, S.R., Hankins, W.B., Westrum, E.F., and Kuskov, O.L. (1998) Heat
282 capacity and thermodynamic properties for coesite and jadeite, reexamination of the quartz-
283 coesite equilibrium boundary. American Mineralogist, 83(3-4), 409-418.
284 Knoche, R., Sweeney, R.J., and Luth, R.W. (1999) Carbonation and decarbonation of eclogites: the
285 role of garnet. Contributions to Mineralogy and Petrology, 135(4), 332-339.
286 Koziol, A.M., and Newton, R.C. (1995) Experimental determination of the reactions magnesite+
287 quartz = enstatite + CO_2 and magnesite = periclase + CO_2, and enthalpies of formation of
288 enstatite and magnesite. American Mineralogist, 80(11-12), 1252-1260.
289 Litasov, K.D., and Shatskiy, A.F. (2019) $MgCO_3$ + SiO_2 reaction at pressures up to 32 GPa studied
290 using in-situ X-ray diffraction and synchrotron radiation. Geochemistry International, 57(9),
291 1024-1033.
292 Luth, R.W. (1995) Experimental determination of the reaction dolomite + 2 coesite = diopside + 2
293 CO_2 to 6 GPa. Contributions to Mineralogy and Petrology, 122(1-2), 152-158.
294 -. (2006) Experimental study of the $CaMgSi_2O_6$-CO_2 system at 3-8 GPa. Contributions to
295 Mineralogy and Petrology, 151(2), 141-157.
296 Martin, A.M., and Hammouda, T. (2011) Role of iron and reducing conditions on the stability of
297 dolomite+ coesite between 4.25 and 6 GPa – a potential mechanism for diamond formation
298 during subduction. European Journal of Mineralogy, 23(1), 5-16.
299 Newton, R.C., and Sharp, W.E. (1975) Stability of forsterite+CO_2 and its bearing on the role of CO_2
300 in the mantle. Earth and Planetary Science Letters, 26(2), 239-244.

Pal'yanov, Y.N., Sokol, A.G., Borzdov, Y.M., and Khokhryakov, A.F. (2002) Fluid-bearing alkaline carbonate melts as the medium for the formation of diamonds in the Earth's mantle: an experimental study. Lithos, 60(3-4), 145-159.

Ragozin, A.L., Shatsky, V.S., Rylov, G.M., and Goryainov, S.V. (2002) Coesite inclusions in rounded diamonds from placers of the Northeastern Siberian Platform. Doklady Earth Sciences, 384(4), 385-389.

Ragozin, A.L., Shatskii, V.S., and Zedgenizov, D.A. (2009) New data on the growth environment of diamonds of the variety V from placers of the Northeastern Siberian platform. Doklady Earth Sciences, 425(2), 436-440.

Schrauder, M., and Navon, O. (1993) Solid carbon dioxide in natural diamond. Nature, 365(6441), 42-44.

Shatskii, A.F., Borzdov, Y.M., Sokol, A.G., and Pal'yanov, Y.N. (2002) Phase formation and diamond crystallization in carbon-bearing ultrapotassic carbonate-silicate systems. Russian Geology and Geophysics, 43(10), 940-950.

Shatskiy, A., Litasov, K.D., Terasaki, H., Katsura, T., and Ohtani, E. (2010) Performance of semi-sintered ceramics as pressure-transmitting media up to 30 GPa. High Pressure Research, 30(3), 443-450.

Shatskiy, A., Borzdov, Y.M., Litasov, K.D., Ohtani, E., Khokhryakov, A.F., Pal'yanov, Y.N., and Katsura, T. (2011) Pressless split-sphere apparatus equipped with scaled-up Kawai-cell for mineralogical studies at 10–20 GPa. American Mineralogist, 96(4), 541-548.

Shatskiy, A., Podborodnikov, I.V., Arefiev, A.V., Minin, D.A., Chanyshev, A.D., and Litasov, K.D. (2018) Revision of the $CaCO_3$–$MgCO_3$ phase diagram at 3 and 6 GPa. American Mineralogist, 103(3), 441-452.

Shirey, S.B., Cartigny, P., Frost, D.J., Keshav, S., Nestola, F., Nimis, P., Pearson, D.G., Sobolev, N.V., and Walter, M.J. (2013) Diamonds and the geology of mantle carbon. Rev Mineral Geochem, 75, p. 355-421.

Smith, E.M., Kopylova, M.G., Frezzotti, M.L., and Afanasiev, V.P. (2015) Fluid inclusions in Ebelyakh diamonds: Evidence of CO_2 liberation in eclogite and the effect of H_2O on diamond habit. Lithos, 216, 106-117.

Sokol, A.G., Borzdov, Y.M., Palyanov, Y.N., and Khokhryakov, A.F. (2015) High-temperature calibration of a multi-anvil high pressure apparatus. High Pressure Research, 35(2), 139-147.

Sokolova, T.S., Dorogokupets, P.I., and Filippova, A.I. (2022) Equations of state of clino-and orthoenstatite and phase relations in the $MgSiO_3$ system at pressures up to 12 GPa and high temperatures. Physics and Chemistry of Minerals, 49(9), 1-14.

Stachel, T., and Luth, R.W. (2015) Diamond formation – Where, when and how? Lithos, 220, 200-220.

Tomilenko, A.A., Ragozin, A.L., Shatskii, V.S., and Shebanin, A.P. (2001) Variation in the fluid phase composition in the process of natural diamond crystallization. Doklady Earth Sciences, 379(5), 571-574.

Vinogradova, Y.G., Shatskiy, A.F., and Litasov, K.D. (2021) Thermodynamic analysis of the reactions of CO_2-fluid with garnets and clinopyroxenes at 3-6 GPa. Geochemistry International, 59(9), 851-857.

This is the peer-reviewed, final accepted version for American Mineralogist, published by the Mineralogical Society of America.
The published version is subject to change. Cite as Authors (Year) Title. American Mineralogist, in press.
DOI: https://doi.org/10.2138/am-2022-8696. http://www.minsocam.org/

Figure captions

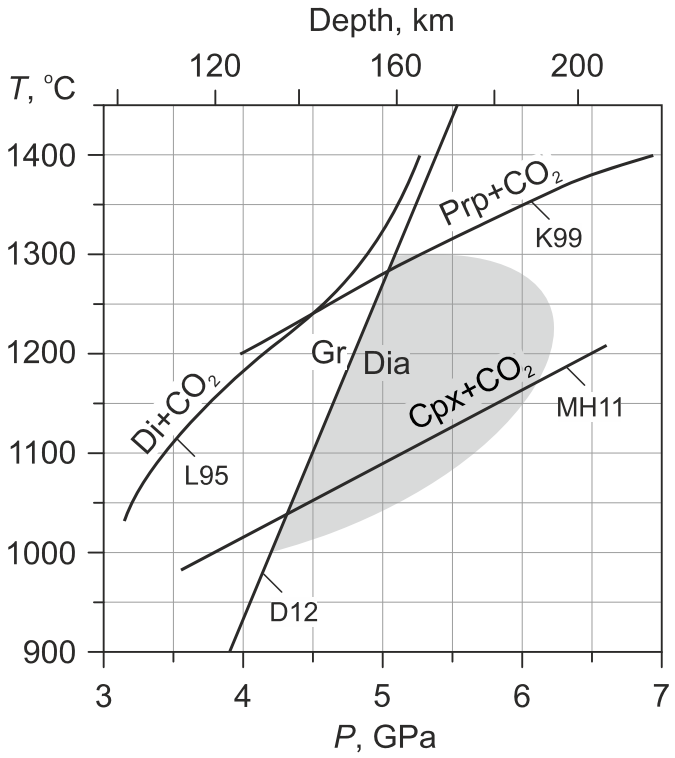

Fig. 1. Carbonation reactions of clinopyroxene and pyrope with CO_2 fluid in comparison with the diamond-to-graphite transition and *P-T* conditions of lithospheric diamond formation (gray area) (Shirey et al., 2013; Stachel and Luth, 2015). L95 – (Luth 1995); K99 – (Knoche et al. 1999), MH11 – (Martin and Hammouda 2011), D12 – (Day 2012). See the nomenclature section for abbreviations.

This is the peer-reviewed, final accepted version for American Mineralogist, published by the Mineralogical Society of America.
The published version is subject to change. Cite as Authors (Year) Title. American Mineralogist, in press.
DOI: https://doi.org/10.2138/am-2022-8696. http://www.minsocam.org/

352

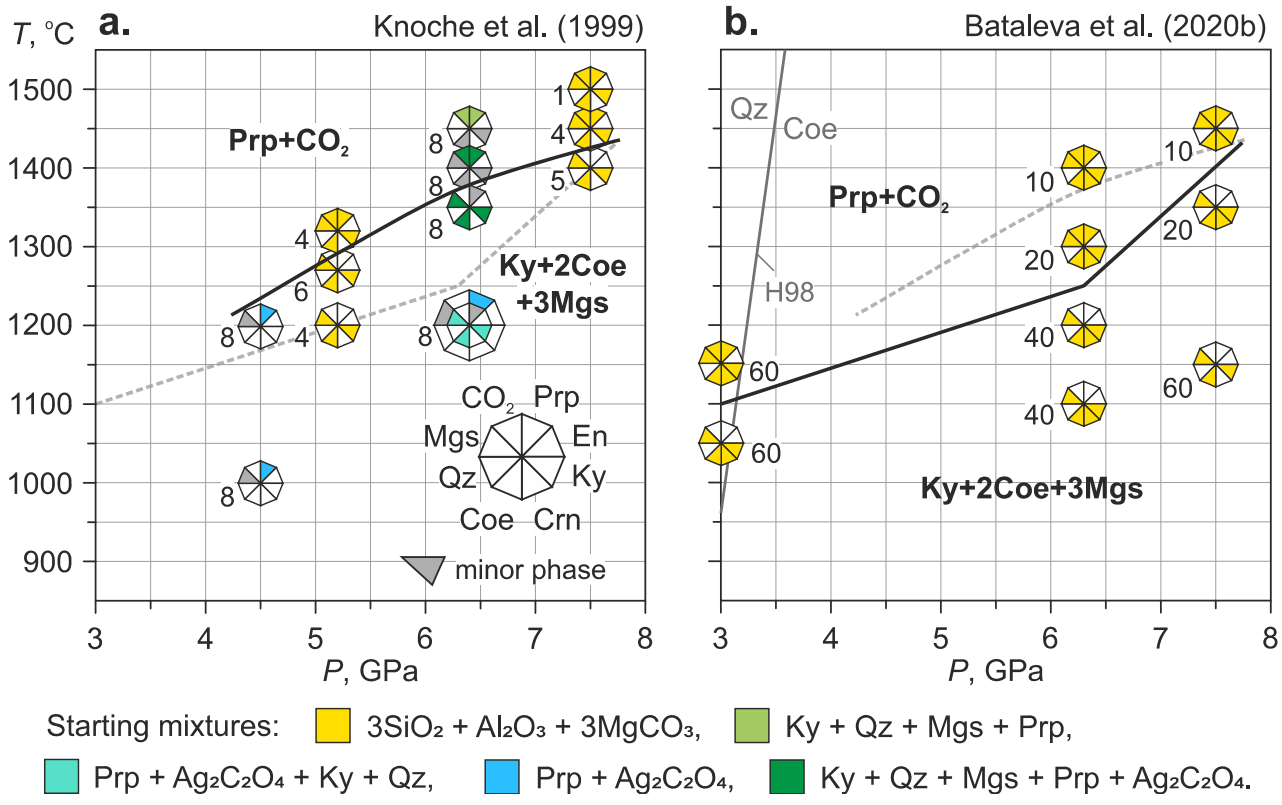

353

354 Fig. 2. Previous experimental data on phase relations in the system pyrope-CO_2 reported by Knoche
355 et al. (1999) (a) and Bataleva et al. (2020b) (b). The numbers near polyhedrons indicate the run
356 duration in hours. H98 – (Hemingway et al. 1998). Please see the Nomenclature section for
357 abbreviations. (Color online)

358

359

360

This is the peer-reviewed, final accepted version for American Mineralogist, published by the Mineralogical Society of America.
The published version is subject to change. Cite as Authors (Year) Title. American Mineralogist, in press.
DOI: https://doi.org/10.2138/am-2022-8696. http://www.minsocam.org/

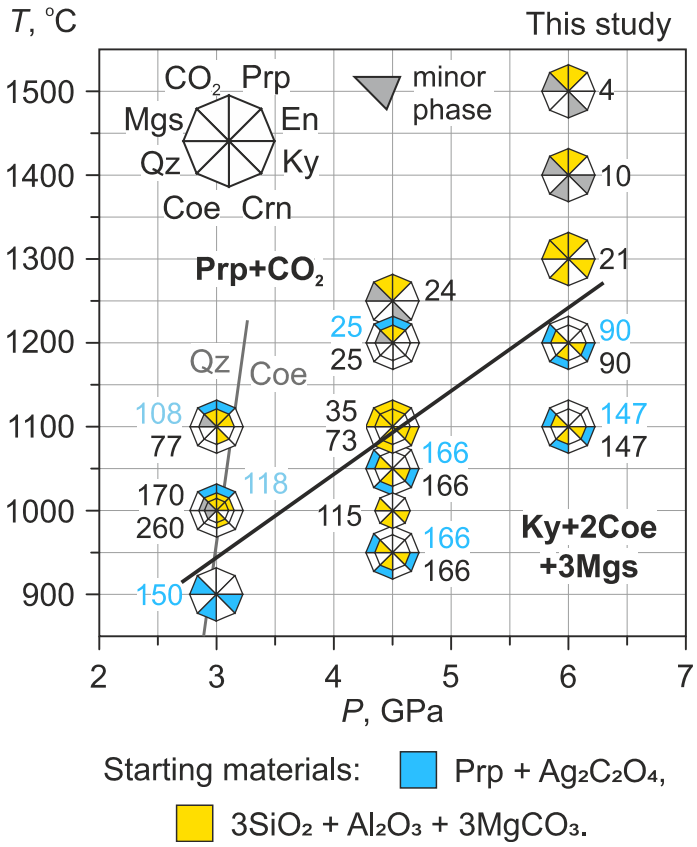

361

362 Fig. 3. Results of experiments on the Prp + $3CO_2$ = Ky + 2Coe + 3Mgs equilibrium boundary. The
363 numbers near polyhedrons indicate the run duration in hours. The quartz-coesite transition is after
364 Hemingway et al. (1998). Abbreviations are given in the Nomenclature section. (Color online)

365

This is the peer-reviewed, final accepted version for American Mineralogist, published by the Mineralogical Society of America.
The published version is subject to change. Cite as Authors (Year) Title. American Mineralogist, in press.
DOI: https://doi.org/10.2138/am-2022-8696. http://www.minsocam.org/

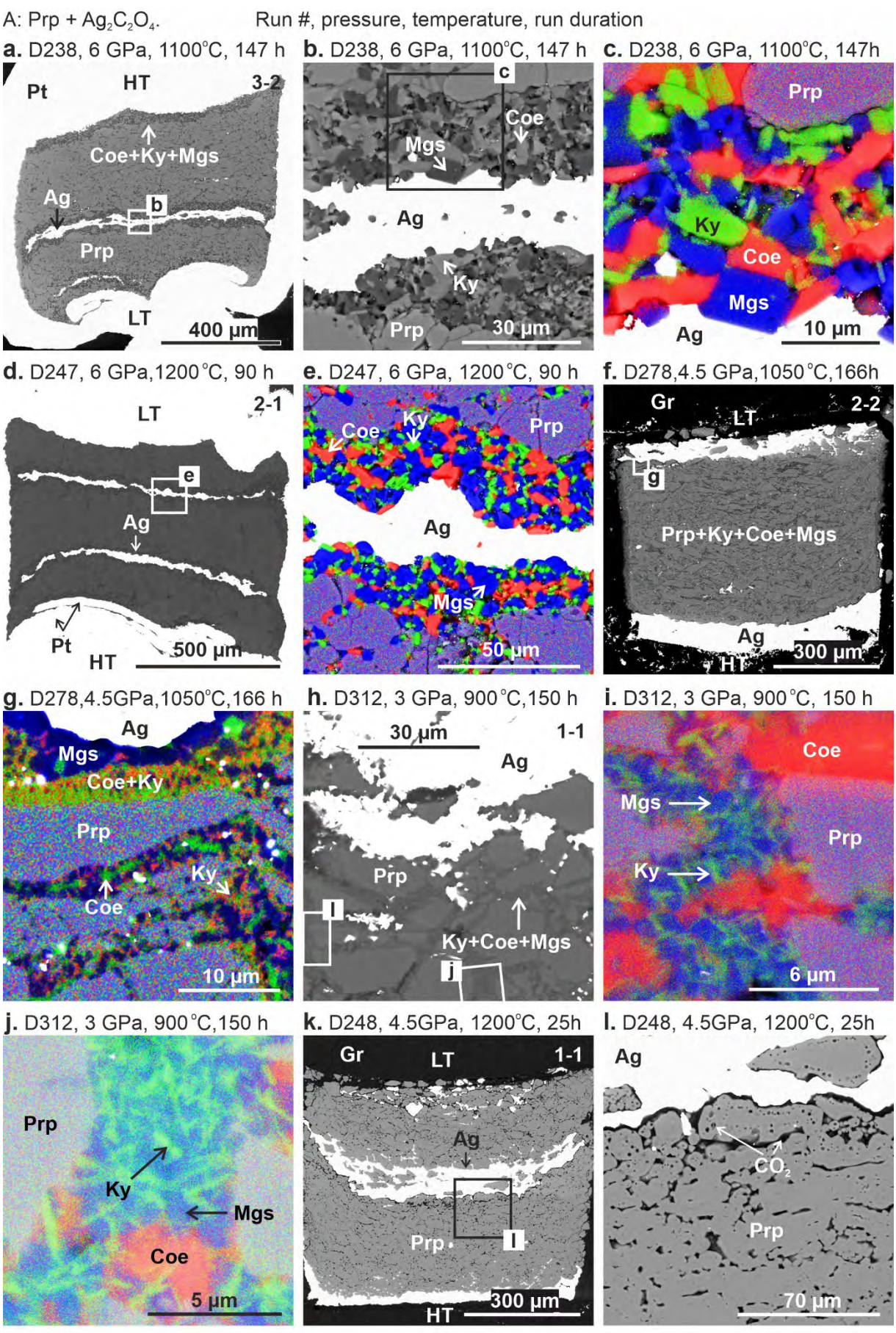

Fig. 4. BSE images of samples recovered from experiments with the pyrope-oxalate starting material (A). HT – high-temperature and LT – low-temperature sample sides. The gravity vector is directed downward. Color images were taken in the element mapping mode. The numbers at the upper right corners of the images with a general view are sample numbers. See the nomenclature section for abbreviations. (Color online)

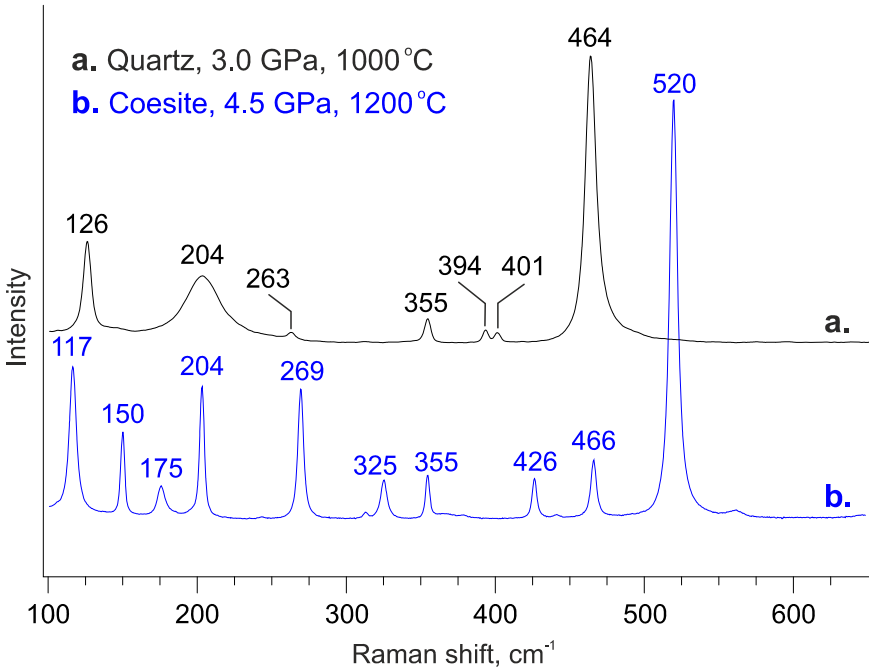

Fig. 5. The Raman spectra of quartz (run D276, 3 GPa, 1000 °C, 170 h) (a) and coesite (run D248, 4.5 GPa, 1200 °C, 25 h) (b).

This is the peer-reviewed, final accepted version for American Mineralogist, published by the Mineralogical Society of America.
The published version is subject to change. Cite as Authors (Year) Title. American Mineralogist, in press.
DOI: https://doi.org/10.2138/am-2022-8696. http://www.minsocam.org/

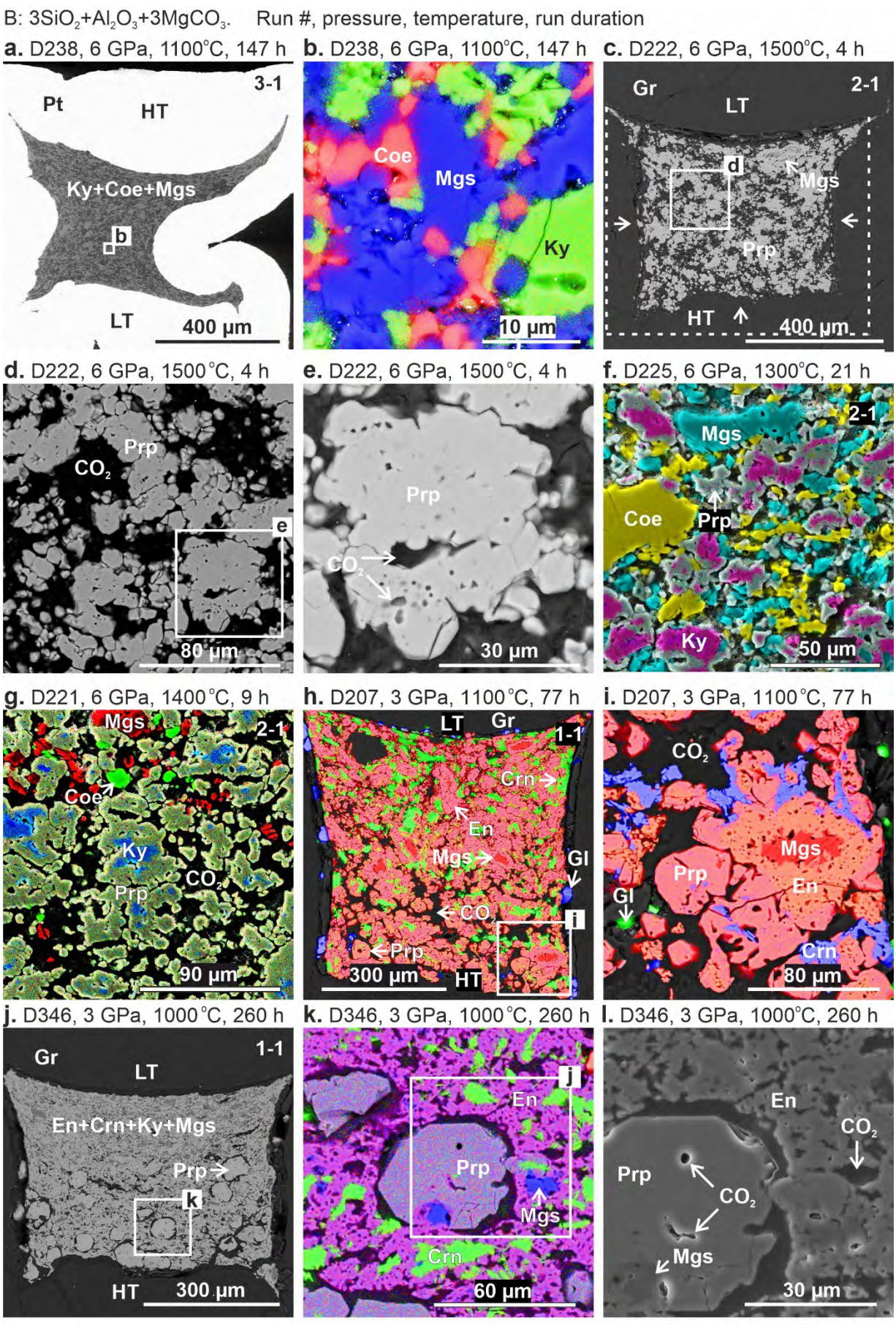

376

This is the peer-reviewed, final accepted version for American Mineralogist, published by the Mineralogical Society of America.
The published version is subject to change. Cite as Authors (Year) Title. American Mineralogist, in press.
DOI: https://doi.org/10.2138/am-2022-8696. http://www.minsocam.org/

Fig. 6. BSE images of samples for the oxide-carbonate starting material (B) $3SiO_2+Al_2O_3+3MgCO_3$. Gl is SiO_2, which remains after sample fixation with gel-type superglue. See the caption of Fig. 4 for further details. (Color online)

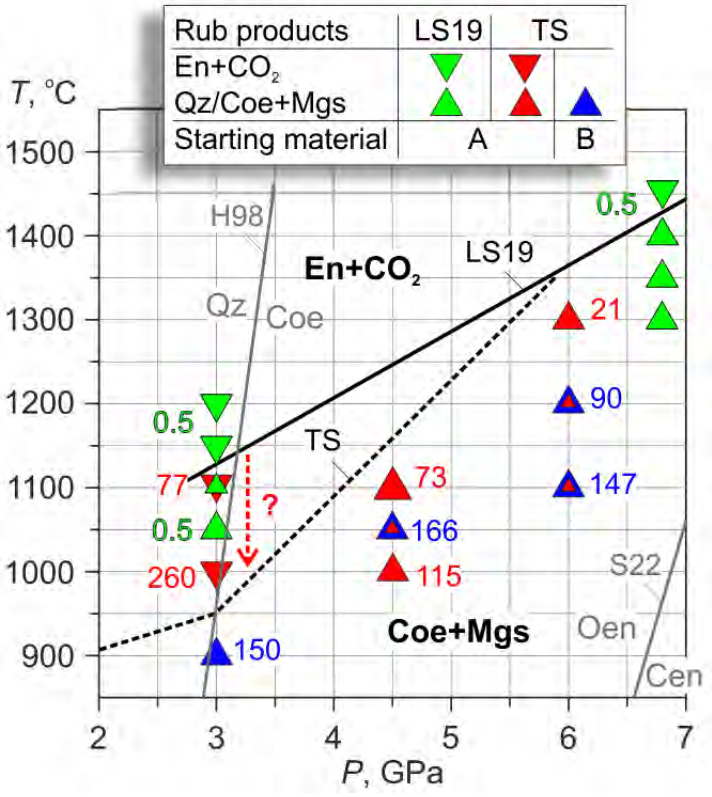

Fig. 7. The enstatite + CO_2 stability field inferred from the present experiments (TS) compared with those by Litasov and Shatskiy (2019) (LS19) obtained using *in situ* synchrotron radiation experiments. The black solid line is the En + $2CO_2$ = 2Coe/Qz + 2Mgs reaction boundary after Litasov and Shatskiy (2019). The dotted line is that the boundary plotted considering present experiments and data of Koziol and Newton (1995). The numbers near triangles indicate the run duration. Oen – orthoenstatite, Cen – clinoenstatite. H98 – (Hemingway et al. 1998), S22 – (Sokolova et al. 2022). (Color online)

This is the peer-reviewed, final accepted version for American Mineralogist, published by the Mineralogical Society of America.
The published version is subject to change. Cite as Authors (Year) Title. American Mineralogist, in press.
DOI: https://doi.org/10.2138/am-2022-8696. http://www.minsocam.org/

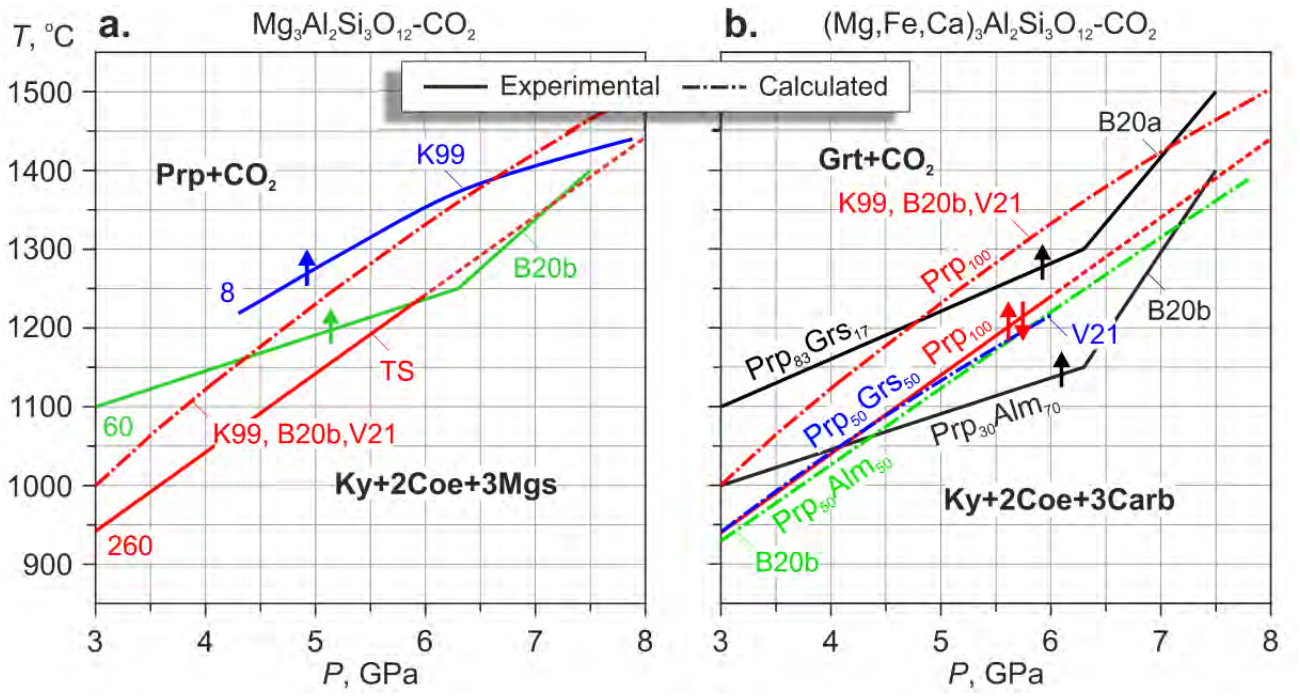

Fig. 8. Intercomparison of this work (TS) with prior experimental (solid lines) and theoretical studies (dash-dotted lines) in the $Mg_3Al_2Si_3O_{12}$-CO_2 (a) and (Mg, Fe, Ca)$_3Al_2Si_3O_{12}$-CO_2 (b) systems. K99 – (Knoche et al. 1999), B20a – (Bataleva et al. 2020a), B20b – (Bataleva et al. 2020b), V21 – (Vinogradova et al. 2021). The numbers indicate the duration of the lowest temperature experiments. The arrows indicate an approach to the reaction boundary from the LT and HT assemblage.

This is the peer-reviewed, final accepted version for American Mineralogist, published by the Mineralogical Society of America.
The published version is subject to change. Cite as Authors (Year) Title. American Mineralogist, in press.
DOI: https://doi.org/10.2138/am-2022-8696. http://www.minsocam.org/

406

407

408

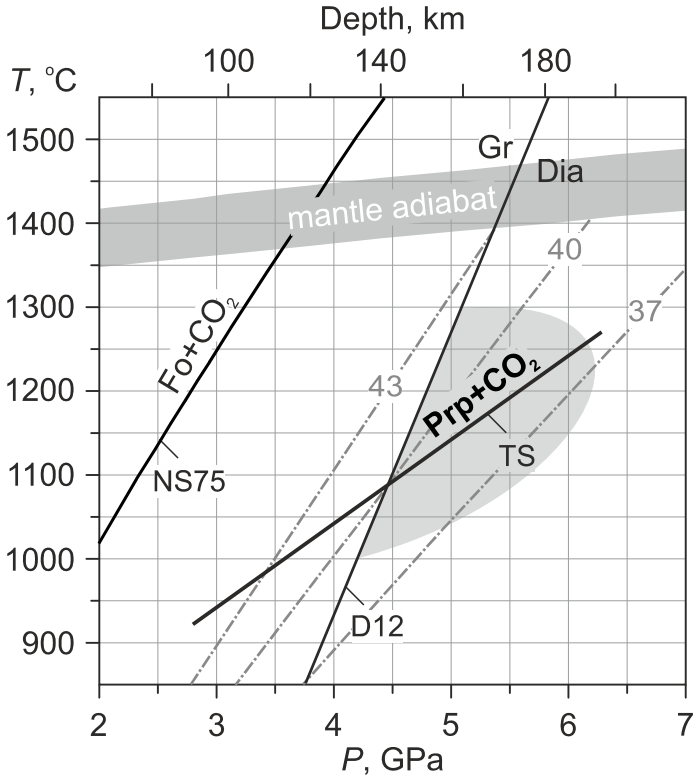

409

410 Fig. 9. The pyrope+CO_2 reaction boundary established in this study (TS) relative to *P*-*T* conditions
411 of diamond formation (gray area) (Shirey et al., 2013; Stachel and Luth, 2015). Dash dotted lines are
412 continental geotherms with potential heat flow of 37, 40, and 43 mW/m^2 after (Hasterok and
413 Chapman 2011). NS75 – (Newton and Sharp 1975), MH11 – (Martin and Hammouda 2011), D12 –
414 (Day 2012).

415

416

417

This is the peer-reviewed, final accepted version for American Mineralogist, published by the Mineralogical Society of America.
The published version is subject to change. Cite as Authors (Year) Title. American Mineralogist, in press.
DOI: https://doi.org/10.2138/am-2022-8696. http://www.minsocam.org/

Table 1. Run conditions and results.

Run#	*P*, GPa	*T*, °C	*t*, h	#	Cap.	S.M.	Run products							
							Prp	En	Ky	Crn	Coe	Qz	Mgs	CO_2
D312	3	900	150	1-1	Gr	A	r	–	+	–	+	–	+	–
D249	3	1000	118	1-4	Gr	A	+	–	–	–	–	–	–	+
D276	3	1000	170	2-3	Gr	B	+	+	–	+	–	r	r	+
D346	3	1000	260	1-1	Gr	B	+	+	+	+	–	–	r	+
D207	3	1100	77	1-1	Gr	B	+	+	–	+	–	r	r	+
D275	3	1100	108	2-1	Gr	A	+	–	–	–	–	–	–	+
D274	4.5	950	166	3-1	Gr	B	–	–	+	–	+	–	+	–
				4-1	Gr	A	r	–	+	–	+	–	+	–
D234	4.5	1000	115	1-1	Gr	B	–	–	+	–	+	–	+	–
D278	4.5	1050	166	3-3	Gr	B	–	–	+	–	+	–	+	–
				2-2	Gr	A	r	–	+	–	+	–	+	–
D226	4.5	1100	35	1-1	Gr	B	+	–	+	–	+	–	+	+
D233	4.5	1100	73	1-1	Gr	B	+	–	+	–	+	–	+	+
D248	4.5	1200	25	3-1	Gr	B	+	–	–	–	–	–	r	+
				1-1	Gr	A	+	–	–	–	–	–	–	+
D219	4.5	1250	24	1-1	Gr	B	+	–	–	r	–	–	r	+
D238	6	1100	147	1-1	Gr	B	–	–	+	–	+	–	+	–
				3-1	Pt	B	–	–	+	–	+	–	+	–
				3-2	Pt	A	r	–	+	–	+	–	+	–
D247	6	1200	90	3-1	Gr	B	–	–	+	–	+	–	+	–
				2-1	Pt	A	r	–	+	–	+	–	+	–
D225	6	1300	20.5	2-1	Gr	B	+	–	+	–	+	–	+	+
D221	6	1400	9.5	2-1	Gr	B	+	–	r	–	r	–	r	+
D222	6	1500	4	2-1	Gr	B	+	–	–	r	–	–	r	+

Notes: *t* – run duration, # – sample number, S.M. – starting material, A – pyrope-oxalate, B – oxide-carbonate ($3SiO_2+Al_2O_3+3MgCO_3$), '+' – phase is present, '–' – phase is absent, r – relict. Please see the Nomenclature section for abbreviations.